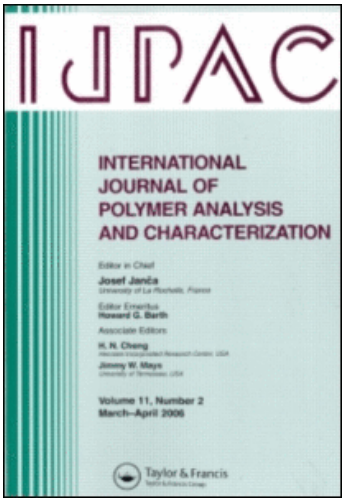

International Journal of Polymer Analysis and Characterization
Publication details, including instructions for authors and subscription information:
http://www.informaworld.com/smpp/title~content=t713646643

Evidence for Generation of Delocalized Polarons in Conducting Polyaniline: A Raman Scattering Spectroscopy Approach

Natalia Gospodinova[a]; Samuel Dorey[a]; Anela Ivanova[a]; Hristina Zhekova[b]; Alia Tadjer[b]
[a] Institut de Chimie des Surfaces et Interfaces, Ecole Nationale Superieure de Chimie de Mulhouse, Mulhouse, France [b] Faculty of Chemistry, University of Sofia, Sofia, Bulgaria

To cite this Article Gospodinova, Natalia , Dorey, Samuel , Ivanova, Anela , Zhekova, Hristina and Tadjer, Alia(2007) 'Evidence for Generation of Delocalized Polarons in Conducting Polyaniline: A Raman Scattering Spectroscopy Approach', International Journal of Polymer Analysis and Characterization, 12: 3, 251 — 271
To link to this Article: DOI: 10.1080/10236660701266963
URL: http://dx.doi.org/10.1080/10236660701266963

International Journal of Polymer Anal. Charact., 12: 251–271, 2007

ISSN: 1023-666X print
DOI: 10.1080/10236660701266963

Taylor & Francis
Taylor & Francis Group

Evidence for Generation of Delocalized Polarons in Conducting Polyaniline: A Raman Scattering Spectroscopy Approach

Natalia Gospodinova, Samuel Dorey, and Anela Ivanova
Institut de Chimie des Surfaces et Interfaces, Ecole Nationale Superieure de Chimie de Mulhouse, Mulhouse, France

Hristina Zhekova and Alia Tadjer
Faculty of Chemistry, University of Sofia, Sofia, Bulgaria

Abstract: Photoexcitation as a novel route for obtaining delocalized polarons in conducting polyaniline is predicted theoretically and confirmed experimentally. Original model experiments and theoretical calculations on protonated emeraldine species with various chain alignments as well as of isolated chains were carried out. In addition, experimental models matching theoretical models of isolated and bulk polyaniline (PANI) chains were synthesized and their absorption and Raman spectra recorded. The detection of the photoexcited states was performed by conventional Raman scattering spectroscopy (generally employed for studying ground states), which is an attractive alternative for generating and characterizing photoexcited delocalized polarons in polyaniline. The occurrence of photoexcited delocalized polaronic species is favored by chain stacking.

Keywords: Photogeneration of polarons; Polyaniline; Raman spectroscopy

The work was partially supported by the COST project P12-"Structuring of polymers" in the framework of COST-STSM-P12-00241 (S.D.) to the University of Sofia and by Project BY-X-202/2006 MON, Bulgaria.

Address correspondence to Natalia Gospodinova, Institut de Chimie des Surfaces et Interfaces, Ecole Nationale Superieure de Chimie de Mulhouse, Mulhouse, France. E-mail: N.Gospodinova@uha.fr

INTRODUCTION

Interaction between polyaniline (PANI), a conjugated conducting polymer, and visible light is still not fully elucidated. It is well known that electronic absorption spectra of conducting PANI (emeraldine salt) obtained by conventional chemical or electrochemical polymerization are characterized by an intensive transition in the visible range ($\lambda_{max} \sim 800$ nm). This state is referred to as primary doped polyaniline.[1] Upon the so-called secondary doping, caused by mixing of the nonconducting emeraldine base form of PANI with camphore- or dodecylbenzenesulfonic acids in the presence of m-cresol, the absorption maximum is shifted further to the near infrared region (NIR) (λ_{max} from $\sim$1200 to ≥ 2600 nm) accompanied by conductivity enhancement of about two orders of magnitude. The nature of these transitions is widely discussed: the visible absorption is attributed to localized polarons and the NIR transitions are often related to delocalized polaronic excitations.[1–4] Speculation is that the former originate from protonation of the iminonitrogens in emeraldine base and the latter are due to structure rearrangement of the polymer chains, e.g., transition from coil-like to extended chain conformation upon secondary doping.[1–4] The two types of polarons are deemed responsible for the electron transport in conducting PANI. It is claimed that the localized polaronic form prevails in shorter phenyl- or amino-capped oligomers,[5] while the ground state multiplicity of longer species remains questionable. The existence of polaronic (magnetically active) states is evidenced by numerous measurements of PANI electron paramagnetic resonance (EPR) spectra.[6] However, the structure of these two types of PANI polarons has not been addressed at the atomic level so far. Apparently, at least two factors govern the generation of delocalized (mainly high-spin) polarons in emeraldine: degree of protonation and stacking (pattern of chain alignment).

Additional evidence for the importance of the pattern of chain alignment offers the treatment of PANI emeraldine base films cast from solution in N-methylpyrrolidinone and stretched at 80°C with aqueous HCl solution (a typical primary doping procedure).[3] This leads to growth of PANI conductivity, which is analogous to the effect of secondary doping.

It is straightforward to analyze the nature of the polaronic states by means of photoexcitation techniques. A number of studies have tackled the photoexcitation of the nonconducting emeraldine (semi-oxidized) and pernigraniline (fully oxidized) base forms of polyaniline.[7–11] They report nearly steady-state photoinduced absorption spectra or light-induced ESR results of short-lived polaronic photoexcited states. To our knowledge, there are few communications presenting long-time (3 h at 10 K) weak photoinduced infrared-active vibrational mode detection

of localized polaronic excited states in pernigraniline base.[10,11] If the nonconducting forms can be photoinduced to conducting ones, then the same route should be even more operative for the emeraldine salt, i.e., the effect of secondary doping could be achieved by photoexcitation.

In an attempt to mimic emeraldine salt behavior we performed theoretical simulations on partially and fully protonated emeraldine tetramers. In order to account for secondary doping factors, various chain alignments are considered and the results are compared to those for isolated chains. The optical parameters of the model systems will elucidate the alternatives for interaction between PANI and light. In parallel, experimental models of isolated and bulk PANI chains are synthesized and their absorption and Raman spectra recorded.

The Raman scattering technique relies on irradiation with fixed-wavelength visible laser beams and simultaneous detection of Raman vibrational fingerprints. Currently, Raman spectra of polyaniline are interpreted in terms of Raman resonance scattering based on the idea of selective vibrational mode enhancement upon coincidence of the absorption maximum of a given chromophore group with the irradiating laser line.[12–19] The frequency range 1300–1400 cm^{-1} is usually associated with the polaron lattice ($C-N^{\circ+}$ stretching). Bands in the interval 1390–1400 cm^{-1} are specifically attributed to vibrational frequencies of delocalized polarons featured by extended emeraldine salt chains resulting from conventional secondary doping.[13]

Herein, Raman scattering will be used to provide an efficient route for studying photoinduced delocalized polarons in conducting PANI at ambient conditions. It should be noted that a concomitant fluorescence emission may be anticipated to accompany the recorded vibrational spectra.[20] A quenching technique will be utilized to suppress the fluorescence contribution.

EXPERIMENTAL SECTION

Synthesis and Characterization of PANI Samples

Reagent-grade aniline and ammonium peroxydisulfate were purchased from Aldrich and used as received. Mica sheets, Artikel G250–1 (MP/GSI), were treated ultrasonically for 5 min in ethanol and dried in nitrogen flow. The oxidative polymerization of aniline was carried out with 10 mL of aqueous solution of aniline (8.8×10^{-2} mol/L) in the presence of 1.5 M HCl and oxidant (8.8×10^{-2} mol/L $(NH_4)_2S_2O_8$) at 0°C in the presence of mica templates. After polymerization the PANI-mica sheets were removed, rinsed with 1.5 M HCl aqueous solution, treated

ultrasonically for 5 min in 1.5 M HCl aqueous solution, and dried at ambient conditions.

The morphology and layer thickness of PANI adsorbed on the mica sheets were determined by atomic force microscopy (AFM) (Digital Instruments MultiMode TM SPM NanoScope IV controller) step height measurement on a scratched sample. According to these data the thickness of the layer formed by closely packed uniform (20 nm in diameter) spherical particles is also 20 nm, i.e., it is a monomolecular layer.

Suspension of PANI single-molecule nanoparticles (SMNP; diameter of $\sim$3 nm) was obtained as described previously.[21] PANI thus prepared was characterized by UV/vis/NIR spectra. Films were cast on Si wafers and used for Raman spectroscopic investigation.

Raman scattering spectra of PANI-on-mica and SMNP-on-Si-wafers were obtained using a LabRam Yobin-Yvon (Horiba) Raman spectrometer with CCD detector and a two-grating (600 and 1800 grooves/mm) monochromator. The device was equipped with an Olympus microscope. Short working-length objectives, 50× and 100×, with respective numerical apertures of 0.5 and 0.9 and three confocal pinholes (400, 600, and 1000 μm) were employed. Frequency-doubled Nd-YAG and He-Ne lasers ($\lambda = 532.1$ nm and $\lambda = 632.8$ nm respectively) were used as sources of excitation irradiation, with laser power between 0.42 μW and 5.0 mW. UV/vis/NIR spectra of SMNP-suspension and PANI-on-mica sheets were recorded with a Beckman DU640 spectrophotometer. All spectral measurements were made at room temperature.

Computational Protocol

All studied emeraldine models were enclosed in a TIP3P water periodic box.[22] The details are provided in Table I. Chloride anions were used as counterions for the positively charged tetramers to achieve overall electro-neutrality of the system. A combined Monte Carlo/molecular mechanics technique was employed for low-energy structure sampling.

Table I. Monte carlo simulation parameters for the studied emeraldine tetramer clusters

No. of tetramers	Protonation degree	No. of water molecules	Box size, Å	Cutoff radii, Å (inner/outer)
1	1^+	125	$14 \times 14 \times 30$	3/72
2	1^+	250	$18 \times 18 \times 30$	5/9
1	2^+	197	$18 \times 18 \times 30$	5/9
2	2^+	394	$20 \times 20 \times 35$	6/10

The hydrated PANI tetramers were subjected to Monte Carlo simulation based on the Metropolis scheme[23] for acceptance of low-energy configurations. The energy of the structures was calculated with the AMBER96 force field.[24] All water molecules were explicitly included in the structure calculation. The original parameters of the AMBER96 force field were augmented with a nonstandard bonding parameter for the CB-CD bonds during the molecular mechanics simulation, with equilibrium bond length $l_0 = 1.46$ Å and force constant of the bond $334\,cm^{-1}$. (Adopted from AM1 results averaged on a series of similar structures in order to reproduce properly the structure of quinoid rings).

This is necessary for proper reproduction of the structure of the quinoid rings, not included in the original force field. This is a standard procedure in force field methods. A switched cutoff[25] with inner radius of 5 Å and outer radius of 9 Å was applied to the non-bonded interactions. The electrostatic interactions used the same cutoff and were calculated in the monopole approximation. The 1–4 electrostatic interactions are scaled by 0.833; the "dielectric constant" is not scaled when calculating the electrostatic interactions. Atomic charges for PANI and aniline were adopted from Mulliken analysis of the AM1 optimized molecules in vacuum, either with singlet or triplet multiplicity in the fully protonated case. Although the use of HF/6-31G* RESP derived charges is recommended by the authors of AMBER, and the use of other density-partitioning schemes has some disadvantages (e.g., the electrostatic interactions are overestimated), we do not think that the use of the Mulliken charge distribution will lead to incorrect results in this case, since we compare tendencies between similar structures. An additional reason to choose the Mulliken atomic charges is our attempt to preserve the balance in our model, which combines methods from two different levels of theory. The employment of electrostatic potential (ESP) derived charges as the initial guess would be even more "unnatural" for AM1 in the second stage of the calculations (simulation of spectral behavior), which could result in incorrect molecular orbits (MOs) and qualitatively wrong absorption spectra—the main and final goal of this study. Therefore, we have decided to use the Mulliken partitioning scheme as an acceptable compromise. A unit negative charge was assigned to each chloride anion, which is a reasonable assumption with respect to the large distances (≥ 3 A) of the counterions from the main chain and their complete hydration. Moreover, the aqueous HCl introduced experimentally is already dissociated.

The electrostatic interactions were calculated in the monopole approximation. Standard AMBER scaling factors were used.[24] The employed version of the force field is applicable for simulations of conjugated organic molecules and is parametrized for the essential fragments present in PANI. In addition, the suitability of the computational

protocol in general and of AMBER96 in particular for calculations on PANI has been validated in previous studies[26] by comparison of the obtained structural parameters with those reported at other theoretical levels.

After equilibration of the Monte Carlo simulations (from 20 000 to 80 000 steps), a series of lowest-energy configurations (from 15 to 20 depending on the cluster) were selected from each Monte Carlo trajectory for further optimization and characterization. The geometry of every series of lowest-energy clusters was fully optimized (PANI and water) with AMBER96. The optimized structures were used for structural analysis and optical spectra simulation. The absorption spectra were calculated for the set of PANI tetramer and counterions only. The aqueous environment was treated as a fixed point-charge enveloping field in spectra computation. The UV/vis spectra were obtained with AM1/CIS(10,10) for isolated and AM1/CIS(20,20) for stacked PANI chains.[25] The above abbreviations mean that the active space comprised 10/20 electrons in 10/20 π-molecular orbitals. The size of the active space was selected on the basis of two criteria: lack of MO degeneracy at the terminal orbitals and inclusion of the same number of π-orbitals in the simulations. The above active spaces satisfy the non-degeneracy requirement and involve 10/20 PANI π-MOs in the spectra simulations of hydrated single/stacked tetramers.

Although the electron correlation is somewhat overestimated by AM1/CI due to the parametrization fitted to reproduce experimental properties at the super critical fluid (SCF) level, it still provides correct trends in the UV/vis optical properties at the expense of acceptable computational time. Moreover, AM1/CI has proven to reflect adequately the experimental UV/vis spectra of some conjugated π-systems of similar nature.[27]

RESULTS AND DISCUSSION

The theoretically designed models include singly (SPE) and doubly (DPE) protonated emeraldine tetramers (Figure 1(A), (B1), (B2)). Protonation leads to redistribution of the electron density, which may preserve the singlet multiplicity of emeraldine base or produce higher spin states such as triplets, quintets, etc., where some spin density is localized in the vicinity of the protonated nitrogens.[28] Figure 1 (structures B1 and B2) offers a schematic representation of the two possible electron and spin-density distributions corresponding to localized (B1) and delocalized (B2) polaronic states in a fully protonated emeraldine tetramer.

SPE and DPE are optimized in vacuum with AM1 Hamiltonian. The obtained structures are used to construct stacks of two species,

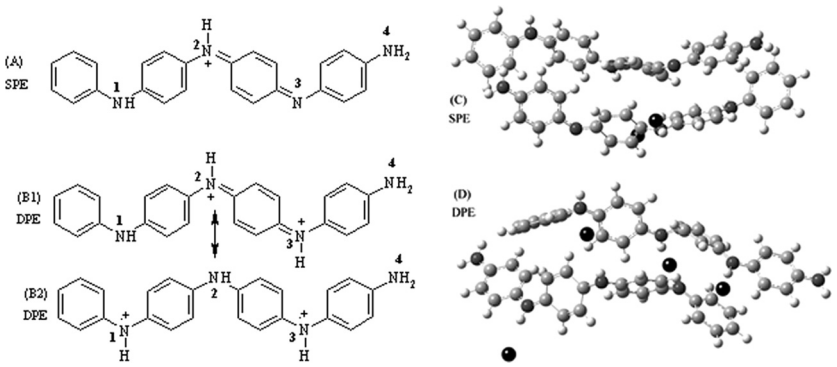

Figure 1. Schemes of (A) singly (SPE) and (B1, B2) doubly (DPE) protonated emeraldine tetramers and AMBER96 optimized geometry of hydrated (C) SPE and (D) DPE stacks; numbering of the nitrogen atoms is provided.

counterions are added, and the clusters are optimized with AMBER96. Various mutual alignments are considered and treated according to the protocol described above. After the Monte Carlo simulation, the sampled snapshots are reoptimized with AMBER96 (an illustrative cluster is shown in (Figure 1(C), (D)). The optical spectra are simulated. The calculated spectra provided in Figure 2(A), (B) are averaged over the reoptimized series.

The experimental spectra used for comparison are taken for 3 nm PANI particles, SMNP (Figure 2(C)), the closest approximation to isolated chains, and for ~20 nm PANI particles layered on mica (Figure 2(D)). The latter case corresponds to the conventional conducting form of polyaniline, the band at $\lambda_{max} \sim 830$ nm being evidence of localized polarons present in the polymer. The graphs in Figure 2(C), (D) reveal that no sign of secondary doped PANI can be traced, whereas even in the isolated DPE tetramers NIR absorption is theoretically predicted. Analogous UV/vis/NIR spectra of primary doped PANI corresponding to Figure 2(D) (but recorded up to 2600 nm)[3] give no bands in the NIR either. The resemblance between the simulated and experimental optical spectra of single molecules looks disputable but the profile is similar. Bearing in mind that chain elongation leads to redshift, the experimental spectra in Figure 2(C) represent oligomers with indefinite degree of protonation and longer than the modeled tetramers in Figue 2(A).

The conclusion that can be drawn from Figure 2 is that chain-stacking both in experimental and in simulated spectra results in redshift of the absorption maxima. On the other hand, PANI obtained directly from standard synthesis is obviously never fully protonated and far from tightly packed (as modeled theoretically). Thus, PANI possessing

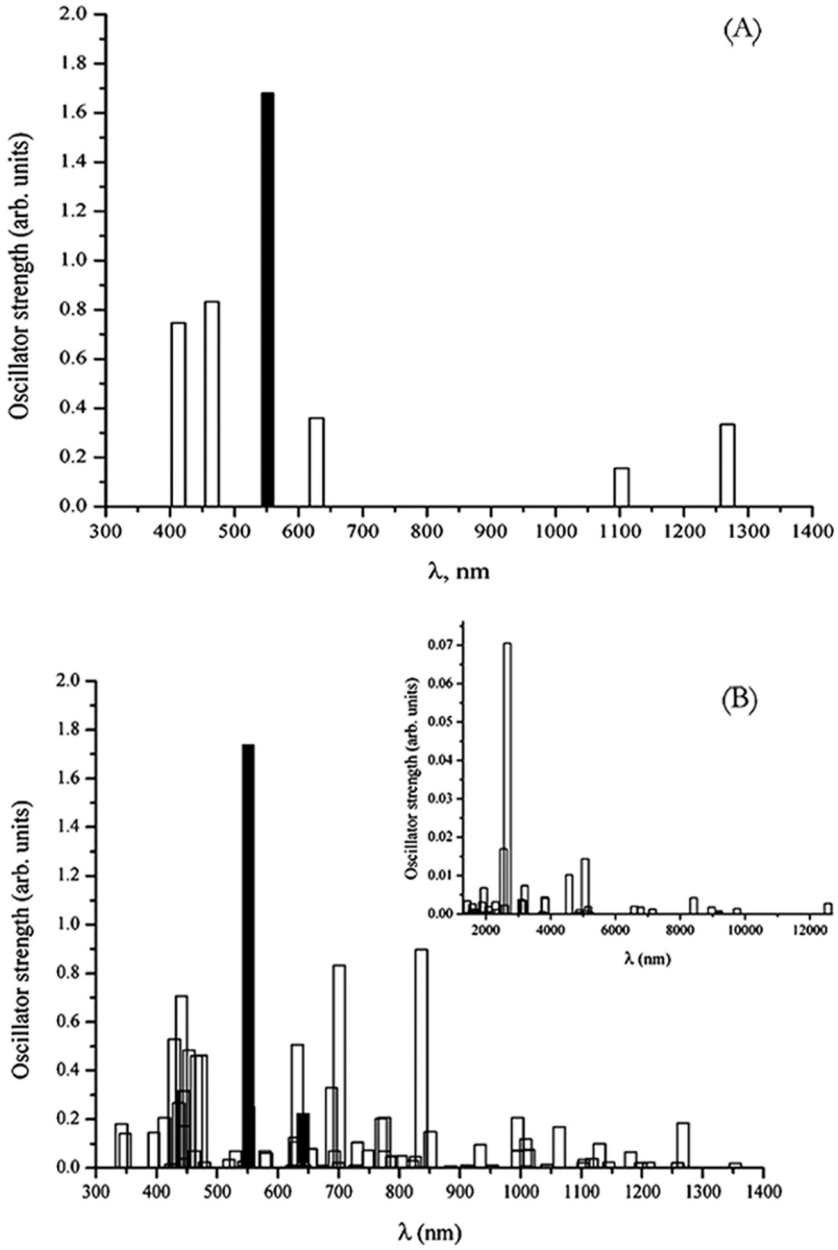

Figure 2. Calculated optical spectra of: (A) hydrated single molecule of SPE (black bar) and DPE (white bars) and (B) hydrated stacks of SPEs (black bars) and DPEs (white bars). Experimental UV/vis/NIR spectra of primary doped (C) SMNP and (D) 20 nm PANI particles layered on mica.

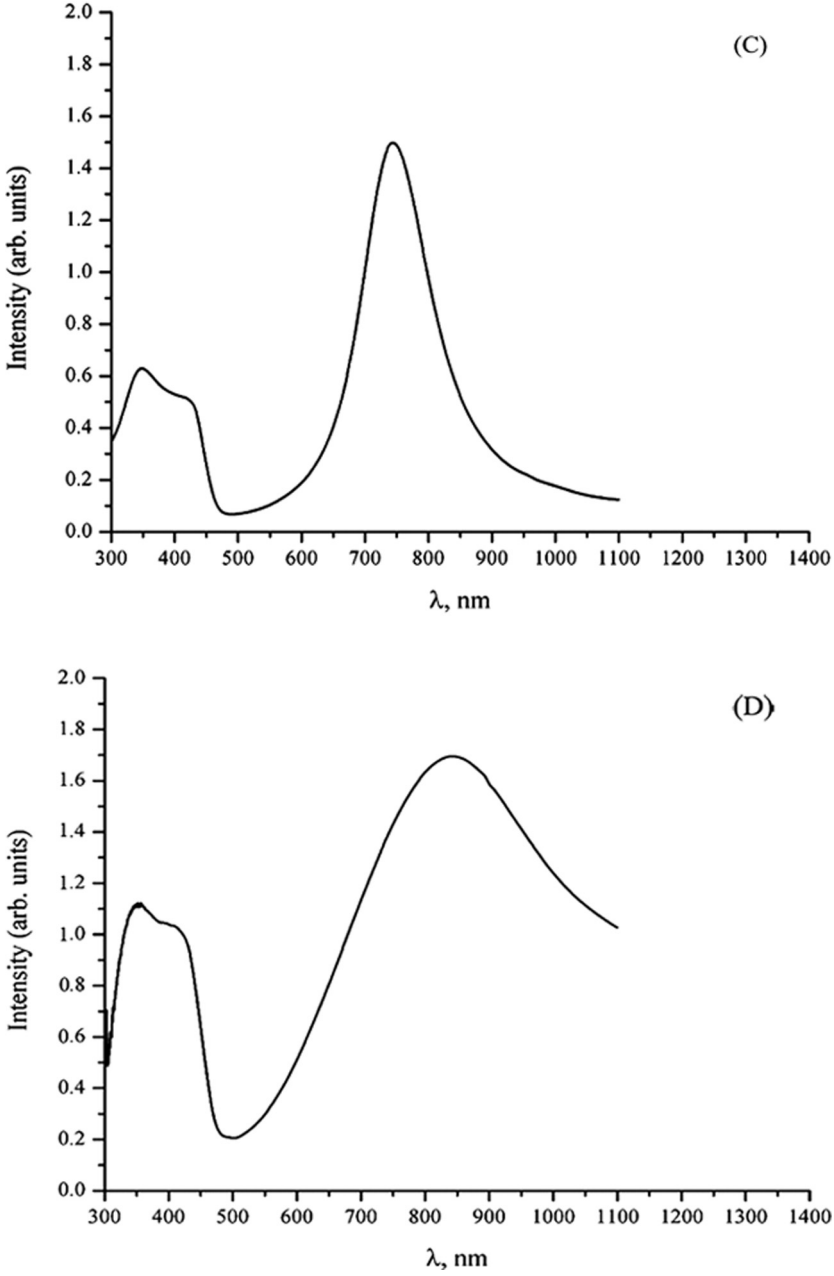

Figure 2. Continued.

well-known fingerprints of delocalized polarons cannot be obtained without additional post-synthesis treatment consisting in rearrangement of the polymer chains by stretching or by secondary doping procedures. The latter are probably accompanied by additional protonation too.

The calculated longest-wavelength transitions (LWT) and spin-state energy splitting of hydrated tetramers in different degrees of protonation are summarized in Figue 3 (left-hand side). The increase in degree of protonation leads to bathochromic shift in the absorption maximum of a single emeraldine tetramer. An extra factor responsible for this redshift may be the decrease of the energy difference between the lowest lying states of various multiplicities upon protonation. In terms of the states of a single tetramer visualized in Figure 3 (right-hand side), not only Δ_1 is reduced to produce the redshift of the intensive absorption band, but also Δ_3 lessens even to negative values, indicative of coexistence of two multiplicities in the tetramer ground state. The high-spin states then would give rise to numerous transitions in the NIR/IR region. The variety of multiplicities and the range of transition wavelengths are expected to be extended with chain elongation, but we have limited our simulations to the shortest oligomer allowing all degrees of oxidation and protonation.

To test the latter hypothesis, quantum mechanical calculations for the energy separation between the low-spin and high-spin ground state in protonated emeraldine were performed. The energy splittings ($\Delta E_{ST} = E_S - E_T$ or $\Delta E_{TQ} = E_T - E_Q$) between the spin states of single and stacked half- and fully protonated emeraldine tetramers were estimated by calculations of $E_{S(T,Q)}$—the respective AM1/CAS(10,10) energies

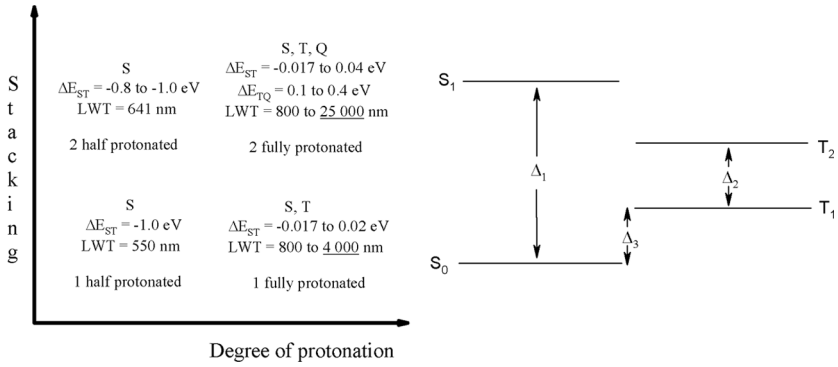

Figure 3. Stacking and protonation effect on spin-state splitting and LWT of emeraldine tetramers (left); energy diagram of the calculated ground and excited states of protonated emeraldine. S_0 (S_1) designate singlet states and T_1 (T_2) the corresponding triplet states. Δ_i (i = 1, 2, 3) are the energy splittings of the spin-states estimated via transition energies (right).

obtained from a single-point complete active space (CAS) computation for the AMBER96 optimized hydrated tetramer structures.[29,30] The energy splitting for the only possible ground states (singlet and triplet) of a single oligomer corresponds to Δ_3 in Figure 3(B). The results define unequivocally singlet ground state for the half-protonated tetramer ($\Delta E_{ST} = -1$ eV), but the triplet and the singlet states are almost degenerate for the fully protonated molecule ($\Delta E_{ST} = 0.02$ eV). Stacking of two fully protonated tetramers in aqueous environment stabilizes the high-spin states (depending on the atomic charge distribution used, $\Delta E_{ST} = -0.017$–0.040 eV, ΔE_{TQ} is in the range 0.1–0.4 eV). AM1/CIS analysis of an ensemble of 270 fully protonated structures reveals that quintet ground state is feasible for 23%, singlet ground state for 11% of the stacks, and triplet ground state for 66% of the clusters. These data confirm the possible spin-states switch upon irradiation with visible light summarized in Figure 3. Depending on the degree of protonation, Δ_3 proves to be positive or negative, and Δ_1 and Δ_2 decrease upon increase of protonation level.

In contrast to DPE, the half-protonated tetramers undergo ~100 nm redshift upon stacking, whereas ΔE_{ST} reduces negligibly. Accordingly, no NIR transitions are witnessed in the simulated spectra. Therefore, the longest wavelength absorptions (from 900 nm to 6000 nm) in Figure 2(B) can be correlated with the experimentally observed free carrier band and correspond to the presence of delocalized polarons in the high-spin species. The more blueshifted excitations ($\lambda < 900$ nm) are thus attributed to the experimental (localized) polaronic bands arising from high population of low-spin excitations. It should be noted that the theoretical model of two stacked fully protonated tetramers does not match completely the molecules present in the experimental samples, where the chains are longer and not necessarily fully protonated, which hinders complete polaron delocalization throughout the chain. However, substructures as the ones modeled theoretically herein are present in the samples, and thus we deem the comparison between the calculated and the experimental spectra appropriate.

Additional evidence for the above speculations is provided by the simulated Raman spectra (Figure 4(A), (B)) of the studied tetramers. The Raman vibrational frequencies were calculated at the RHF/6-31G* and B3LYP/6-31G* levels after full geometry optimization of the respective (half- or fully protonated) PANI tetramer in vacuum.[31] In order to juxtapose to experimental Raman spectra of PANI films, 0.8929 (RHF) and 0.9610 (B3LYP) scaling factors were applied to the theoretical frequencies. The main differences between the theoretical Raman spectra of the half- and fully protonated tetramers are the band sequence in the region 1300–1400 cm^{-1} and the band intensity in the region 1500–1600 cm^{-1}. More important is the former effect, which will be discussed in

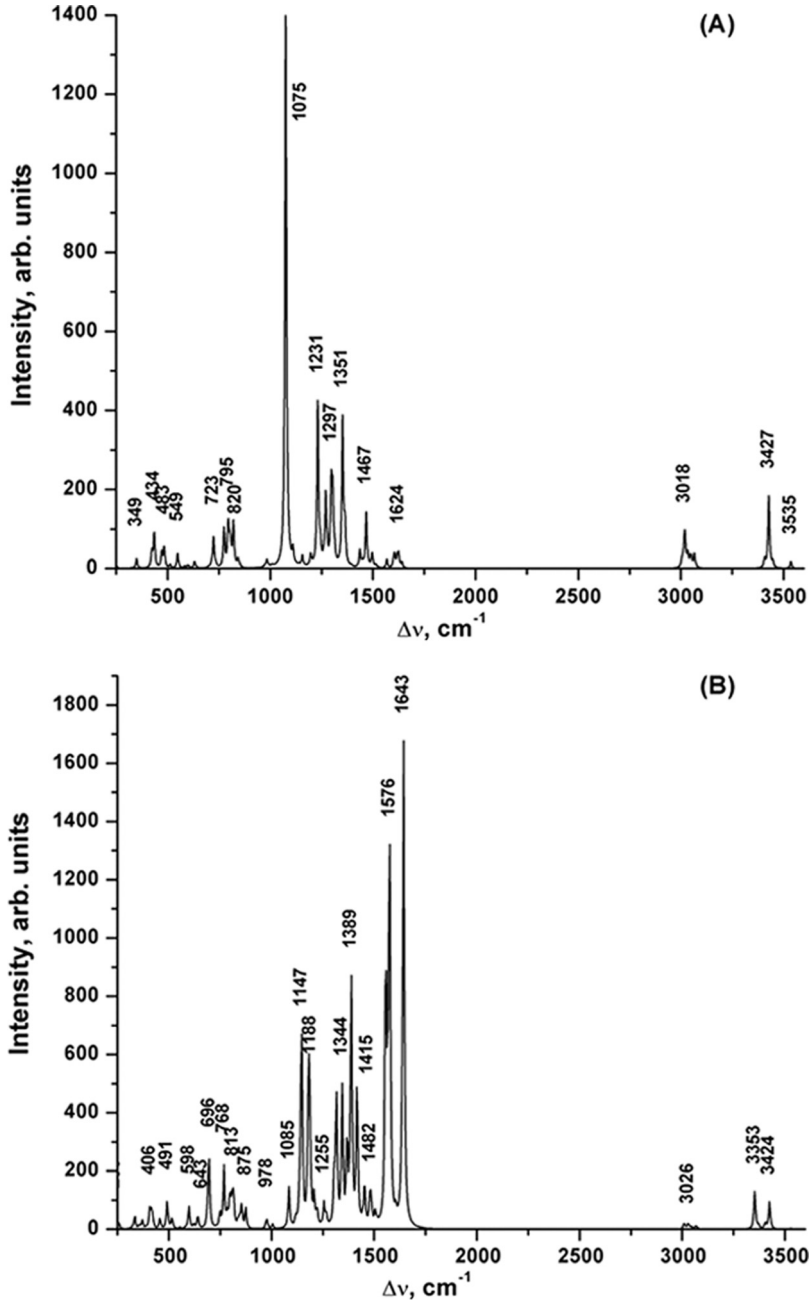

Figure 4. Calculated Raman spectra: RHF/6-31G* of (A) singly and (B) doubly protonated emeraldine tetramer and B3LYP/6-31G* of (C) singly and (D) doubly protonated emeraldine tetramer in vacuum.

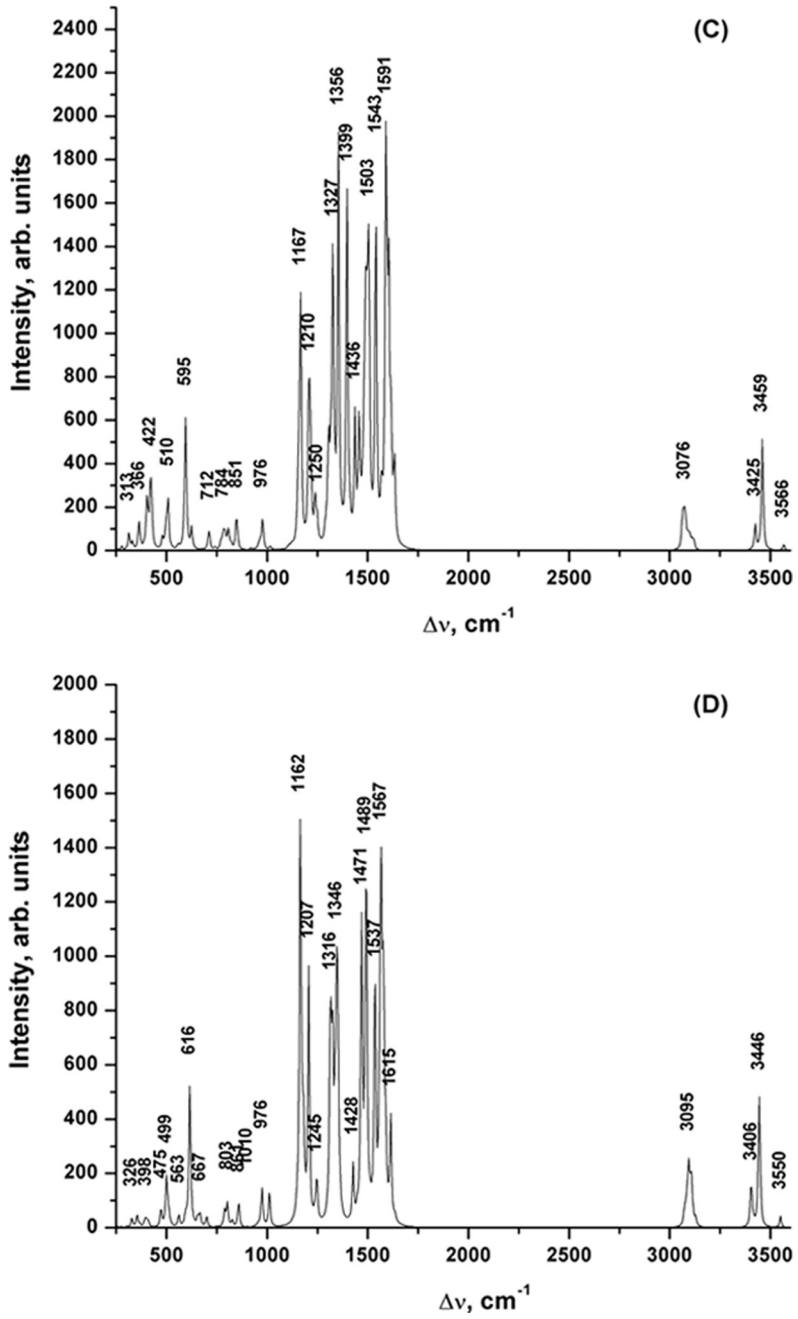

Figure 4. Continued.

detail. The half-protonated molecule features a single RHF/B3LYP vibrational mode at 1351/1399 cm^{-1} and the fully protonated one has three vibrational bands, at 1315/1316 cm^{-1}, 1344/1346 cm^{-1}, and 1389/1326 cm^{-1}. All three of them correspond predominantly to C–N–H mixed with some C–C–H bending. However, those at 1351/1399 cm^{-1} and 1344/1346 cm^{-1} involve only a small portion of the molecule, whereas at the other two the entire core part of the molecule participates in the vibration. Therefore, the bands at 1315/1316 cm^{-1} and 1389/1326 cm^{-1} can be considered as characteristic for delocalized polarons. In the region above 3000 cm^{-1} the simulation results in several low-intensity N–H stretching bands, at 3018/3076 cm^{-1}, 3427/3425 cm^{-1}, and 3535/3459 cm^{-1} for SPE, and at 3026/3095 cm^{-1}, 3353/3406 cm^{-1}, and 3424/3446 cm^{-1} for DPE. The apparent shift of the 3535/3459 cm^{-1} band in SPE to 3353/3406 cm^{-1} in DPE is just due to enhanced N–H stretching of the first ptotonated N-atom (N2) in the presence of the second (N3). Thus, this band cannot be attributed specifically to delocalized polarons. All B3LYP bands are blueshifted with respect to the RHF ones, except for the peak at 1389/1326 cm^{-1}. This is due to milder twisting in the vicinity of the protonated nitrogen atoms yielded by the B3LYP geometry optimization, which affects the energy of this collective vibration. Both simulated Raman spectra are in good agreement with experiment results (Figure 5), the performance of B3LYP being better. In the present work, Raman scattering spectra of emeraldine salt films were measured at ambient temperature in conditions that can enhance or quench photoexcited species and concomitant fluorescence selectively. The factors are the laser line and power; the agent suppressing fluorescence emission by affecting the excited state lifetime is water. The proper balance of experimental conditions allows vibrational fingerprint assessment of photoexcited delocalized polarons in conducting PANI.

The Raman spectra of the investigated PANI species were obtained with two laser lines ($\lambda = 632.8$ nm or 532.1 nm) at various laser powers between 0.42 μW and 5.0 mW at 298 K. The spectra are presented in Figures 5 and 6. The vibrational bands characteristic of conventional PANI[12–19] are observed in all cases, but some differences are witnessed too. Figure 5(A), (B) represents the Raman spectra of SMNP with the two laser lines. In neither of them is the 1390 cm^{-1} band, which is characteristic of delocalized polaronic states,[13] traceable. Assuming that the degree of protonation is the same in the 3 nm and 20 nm particle layers (same pH maintained during synthesis), the major difference is in the possibility of stacking, which is insignificant in SMNP and considerable in the large particles. Judging by the optical spectrum, however, no delocalized polarons are expected to exist in the polymer. Interestingly, the Raman spectra for the 20 nm particle layers with both lasers contain a band at ~1390 cm^{-1} (Figure 6(A), (B)). Since no electronic absorption

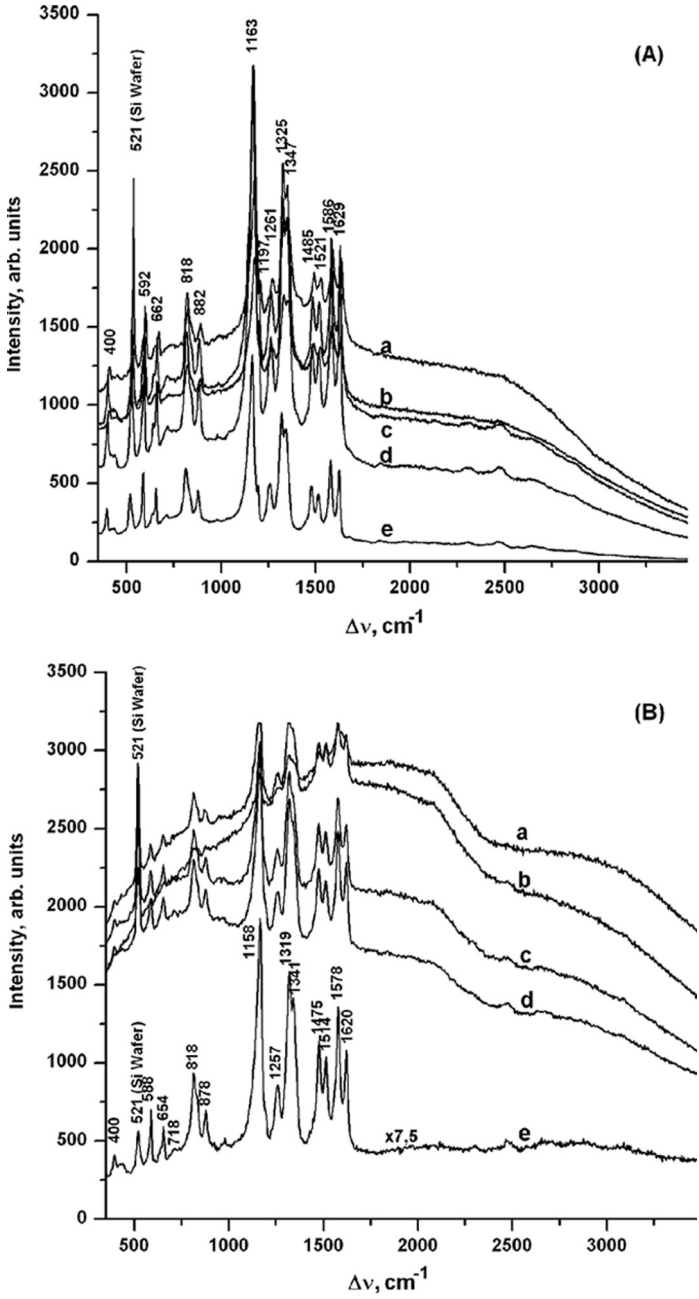

Figure 5. Raman scattering spectra of SMNP cast on Si-wafers at different laser power: (a) 5.0 mW, (b) 2.7 mW, (c) 1.2 mW, (d) 0.5 mW, (e) 0.04 mW; (A) recorded upon $\lambda = 632.8$ nm laser irradiation; (B) recorded upon $\lambda = 532.1$ nm laser irradiation.

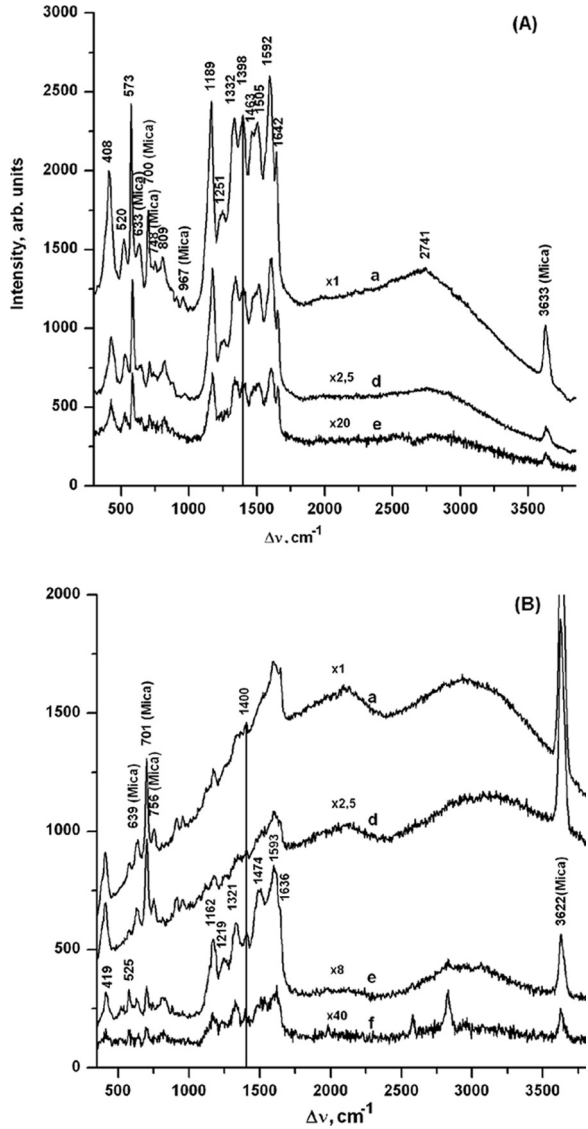

Figure 6. Raman scattering spectra of 20 nm PANI particles layered on mica at different laser power: (a) 5.0 mW, (b) 2.7 mW, (c) 1.2 mW, (d) 0.5 mW, (f) 0.42 μW; spectra (A) and (C) are recorded upon $\lambda = 632.8$ nm laser irradiation; spectra (B) and (D) are recorded upon $\lambda = 532.1$ nm laser irradiation; spectra (C) and (D) are obtained from samples A and B covered with 1.5 M HCl aqueous solution.

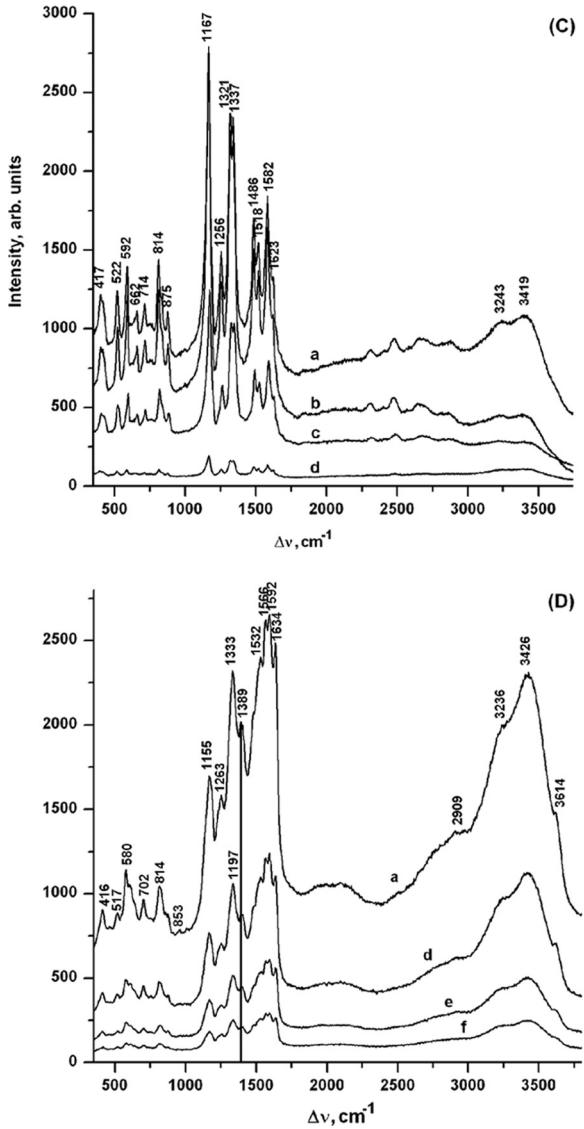

Figure 6. Continued.

transition corresponding to delocalized polaronic states is detected in the samples before laser treating, we assume that delocalized polaronic species are created during the laser irradiation, i.e., they have photoexcited nature. The standard technique for quenching excited states is addition of water. Therefore, a second series of Raman scattering experiments

included covering the PANI layers with a 1.5 M HCl aqueous solution. The HCl was used in order to maintain the conducting emeraldine form of the polymer. The resulting spectra are shown in Figure 6(C), (D).

The effective quenching of the excited states is evidenced by almost complete absence of fluorescence, which also leads to enhanced resolution of the spectra. The band at $\sim$1390 cm^{-1} disappears entirely from the spectrum obtained by irradiation with the lower energy laser, but it remains in the spectrum yielded by higher energy laser irradiation. This confirms the photoexcitation nature of this band. Moreover, it is consistent with the higher population of excited states produced by the higher energy laser. The high-energy laser treatment of primary doped PANI may prove to have the same effect as secondary doping of the samples, i.e., it can increase the amount of charge carriers associated with delocalized polarons and thus improve conductivity. Since laser irradiation is strictly focused, this opens perspectives for further practical applications of photoinduced local conductivity of PANI.

CONCLUSIONS

In summary, the present study addresses the possibility of generation of photoexcited delocalized polarons in conducting polyaniline films.

The problem is accessed both from experimental and theoretical standpoints, the two approaches being designed to match each other as much as possible. A specific synthetic procedure is developed to fabricate small single-molecule PANI nanoparticles ($\sim$3 nm) corresponding to molecular simulations on isolated hydrated emeraldine oligomers. For comparison with synthetically obtained nano-size monolayers of 20 nm PANI particles, models of stacked hydrated oligomers were tailored. The interplay of protonation degree and stacking pattern was monitored and an attempt to rationalize the occurrence of delocalized polarons based on spin-state energy splittings was made, attesting that the interstate gap grows smaller upon protonation and a variety of quasi-degenerate spin states becomes feasible upon stacking. Experimental characterization of the species was achieved by UV/vis/NIR and Raman scattering spectroscopy. Very good agreement between the experimental spectra and the theoretical estimates was obtained.

The data reveal that no delocalized polarons can be induced in SMNP, regardless of the laser wavelength or power. The possibility for generation of conducting delocalized states appears due to intermolecular interactions, illustrated by experimental Raman spectra of 20 nm PANI particles. The different behavior of the layers, depending on the energy of the irradiating light, shows that the effects typical for secondary doping can be triggered by photoexcitation. Thus, light-assisted polaron

redistribution can be used as an alternative to other conductivity-enhancement procedures such as protonic or oxidative doping.

Raman scattering proves to be an efficient nonstandard route for studying photoinduced delocalized polarons in conducting PANI at ambient conditions.

REFERENCES

[1] Saprigin, A. V., K. R. Brenneman, W. P. Lee, S. M. Long, R. S. Kohlman, and A. J. Epstein. (1999). Li^+ doping-induced localization in polyaniline. *Synth. Met.* **100**, 55–59.

[2] Kahol, P. K., R. P. Perera, K. K. Satheesh Kumar, S. Geetha, and D. C. Trivedi. (2003). Electron localization length in polyaniline. *Solid State Commun.* **125**, 369–372.

[3] MacDiarmid, A. G. and A. Epstein. (1995). Secondary doping in polyaniline. *Synth. Met.* **69**, 85–92.

[4] (a) Xia, Y., J. M. Wiesinger, A. G. MacDiarmid, and A. J. Epstein. (1995). Camphorsulfonic acid fully doped polyaniline emeraldine salt: Conformations in different solvents studied by an ultraviolet/visible/near-infrared spectroscopic method. *Chem. Mater.* **7**, 443–445; (b) Min, Y., Y. Xia, A. G. MacDiarmid, and A. J. Epstein. (1995). Vapor phase "secondary doping" of polyaniline. *Synth. Met.* **69**, 159–160.

[5] Baughman, R. H., J. F. Wolf, H. Eckhardt, and L. W. Shaklette. (1989). The structure of a novel polymeric metal: Acceptor-doped polyaniline. *Synth. Met.* **25**, 121–137; Shaklette, L. W., J. F. Wolf, S. Gould, and R. H. Baughman. (1988). Structure and properties of polyaniline as modeled by single-crystal oligomers. *J. Chem. Phys.* **88**, 3955–3961.

[6] (a) Kon'kin, A., V. Shtyrlin, R. Garipov, A. Aganov, A. Zakharov, V. Krinichnyi, P. Adams, and A. Monkman. (2002). EPR, charge transport, and spin dynamics in doped polyanilines. *Phys. Rev. B* **66**, 075203–075213; (b) Krinichnyi, V. I., H.-K. Roth, G. Hinrichsen, F. Lux, and K. Lueders. (2002). EPR and charge transfer in H_2SO_4-doped polyaniline. *Phys. Rev. B* **65**, 155205–155218; (c) Brenneman, K. R., J. Feng, Y. Zhou, A. G. MacDiarmid, P. K. Kahol, and A. Epstein. (1999). EPR of mesoscale polyanilines. *Synth. Met.* **101**, 785–786; (d) Male, R. and R. D. Allendoerfer. (1988). Anodic oxidation of p-aminodiphenylamine: An electron paramagnetic resonance and electrochemical study. *J. Phys. Chem.* **92**, 6237–6240; (e) Langer, J. J., R. Krzyminiewski, Z. Kruczynski, T. Gibinski, I. Czajkowski, and G. Framski. (2001). EPR and electrical conductivity in microporous polyaniline. *Synth. Met.* **122**, 359–362; (f) Hopkins, A. R., P. G. Rasmussen, and R. A. Basheer. (1996). Characterization of solution and solid state properties of undoped and doped polyanilines processed from hexafluoro-2-propanol. *Macromolecules* **29**, 7838–7846.

[7] Roe, M. G., J. M. Ginder, P. E. Wigen, A. J. Epstein, M. Angelopoulos, and A. G. MacDiarmid. (1988). Photoexcitation of polarons and molecular excitons in emeraldine base. *Phys. Rev. Lett.* **60**, 2789–2792.

[8] Sariciftci, N. S., L. Smilowitz, Y. Cao, and A. J. Heeger. (1993). Absorption spectroscopy of nonlinear excitations in polyaniline. *J. Chem. Phys.* **98**, 2664–2669.
[9] Misurkin, I. A., T. S. Zhuravleva, V. M. Geskin, V. Gulbinas, S. Pakalnis, and V. Butvilos. (1994). Electronic processes in polyaniline films photoexcited with picosecond laser pulses: A three-dimensional model for conducting polymers. *Phys. Rev. B* **49**, 7178–7192.
[10] Leng, J. M., R. P. McCall, K. R. Cromack, Y. Sun, S. K. Manohar, A. G. MacDiarmid, and A. J. Epstein. (1993). Photoexcited solitons and polarons in pernigraniline-base polymers. *Phys. Rev. B* **48**, 15719–15731.
[11] Leng, M., R. P. McCall, K. R. Cromack, H. J. Ye, Y. Sun, S. K. Manohar, A. G. MacDiarmid, and A. J. Epstein. (1992). Photoexcitations in pernigraniline: Ring-torsional polarons and bond-order solitons. *Phys. Rev. Lett.* **68**, 1184–1187.
[12] Folch, S., A. Gruger, A. Regis, and P. Colomban. (1996). Optical and vibrational spectra of sols/solutions of polyaniline: Water as secondary dopant. *Synth. Met.* **81**, 221–225.
[13] Pereira da Silva, J. E., M. L. A. Temperini, and S. I. Cordoba de Torresi. (1999). Secondary doping of polyaniline studied by resonance Raman spectroscopy. *Electrochim. Acta* **44**, 1887–1891.
[14] Folch, S., A. Regis, A. Gruger, and P. Colomban. (2000). Chain length effect on intrachain electronic excitation and interchain coupling in poly- and oligo-anilines. *Synth. Met.* **110**, 219–227.
[15] Dufour, B., P. Rannou, J. P. Travers, A. Pron, M. Zagorska, G. Korc, I. Kulszewicz-Bajer, S. Quillard, and S. Lefrant. (2002). Spectroscopic and spectroelectrochemical properties of a poly(alkylthiophene)-oligoaniline hybrid polymer. *Macromolecules* **35**, 6112–6120.
[16] El Khalki, A., A. Gruger, and P. Colomban. (2003). Bulk–surface nanostructure and defects in polyaniline films and fibres. *Synth. Met.* **139**, 215–220.
[17] Wei, Z., Z. Zhang, and M. Wan. (2002). Formation mechanism of self-assembled polyaniline micro/nanotubes. *Langmuir* **18**, 917–921.
[18] Quillard, S., M. Boyer, M. Cochet, J.-P. Buisson, G. Louarn, and S. Lefrant. (1999). Spectroelectrochemical measurements of the conducting form of polyaniline and related oligomers. *Synth. Met.* **101**, 768–771.
[19] Mazeikiene, R., G. Niaura, and A. Malinauskas. (2005). Surface enhanced resonance Raman spectroelectrochemical study of electrochemically generated copolymer films of aniline and aminonaphthalenedisulfonates. *J. Electroanal. Chem.* **580**, 87–93.
[20] Sakai, M. and M. Fujii. (2004). Vibrational energy relaxation of the 7-azaindole dimer in CCl_4 solution studied by picosecond time-resolved transient fluorescence detected IR spectroscopy. *Chem. Phys. Lett.* **396**, 298–302.
[21] Dorey, S., C. Vasilev, L. Vidal, C. Labbe, and N. Gospodinova. (2005). Ultrafine nano-colloid of polyaniline. *Polymer* **46**, 1309–1315.
[22] Jorgensen, W. L., J. Chandrasekhar, J. D. Madura, R. W. Impey, and M. L. Klein. (1983). Comparison of simple potential functions for simulating liquid water. *J. Chem. Phys.* **79**, 926–935.
[23] Metropolis, N., A. W. Rosenbluth, M. N. Rosenbluth, A. H. Teller, and E. Teller. (1953). Equation of state calculations by fast computing machines. *J. Chem. Phys.* **21**, 1087–1092.

[24] (a) Weiner, S. J., P. A. Kollman, D. A. Case, U. C. Singh, C. Ghio, G. Alagona, S. Profeta, Jr., and P. Weiner. (1984). A new force field for molecular mechanical simulation of nucleic acids and proteins. *J. Am. Chem. Soc.* **106**, 765–784; (b) Weiner, S. J., P. A. Kollman, D. T. Nguyen, and D. A. Case. (1986). An all atom force field for simulations of proteins and nucleic acids. *J. Comput. Chem.* **7**, 230–252; (c) Cornell, W. D., P. Cieplak, C. I. Bayly, I. R. Gould, K. M. Merz, Jr., D. M. Ferguson, D. C. Spellmeyer, T. Fox, J. W. Caldwell, and P. A. Kollman. (1995). A second generation force field for the simulation of proteins, nucleic acids, and organic molecules. *J. Am. Chem. Soc.* **117**, 5179–5197.

[25] *HyperChem 7.0 Reference Manual*. (2002). Gainesville, Fla.: Hypercube Inc.

[26] (a) Ivanova, A., G. Madjarova, A. Tadjer, and N. Gospodinova. (2006). Effect of solvation and intermolecular interactions on the structure and optical properties of PANI oligomers. *Int. J. Quant. Chem.* **106**, 1383–1395; (b) Ivanova, A., A. Tadjer, and B. Radoev. (2002). Theoretical study of insoluble polymer monolayers. *Int. J. Quant. Chem.* **89**, 397–404; (c) Ivanova, A., A. Tadjer, and N. Gospodinova. (2006). Theoretical study of the influence of monomer excess on the structure and properties of polyaniline oligomers. *J. Phys. Chem. B* **110**, 2555–2564.

[27] Zoppellaro, G., A. Ivanova, V. Enkelmannn, A. Geies, and M. Baumgarten. (2003). Synthesis, magnetic properties and theoretical calculations of novel nitronyl nitroxide and imino nitroxide diradicals grafted on terpyridine moiety. *Polyhedron* **22**, 2099–2110.

[28] Grossmann, B., J. Heinze, T. Moll, C. Palivan, S. Ivan, and G. Gescheidt. (2004). Electron delocalization in one-electron oxidized aniline oligomers, paradigms for polyaniline. A study by paramagnetic resonance in fluid solution. *J. Phys. Chem. B* **108**, 4669–4672.

[29] Stewart, J. J. P. (1995). *MOPAC: A General Molecular Orbital Package, Version 7.2*. Bloomington, Ind.: QCPE.

[30] Karabunarliev, S., M. Baumgarten, and K. Müllen. (1998). Crossover to an even-parity lowest excited singlet in large oligorylenes: A theoretical study. *J. Phys. Chem. A* **102**, 7029–7034.

[31] Frisch, M. J., G. W. Trucks, H. B. Schlegel, G. E. Scuseria, M. A. Robb, J. R. Cheeseman, J. A. Montgomery, Jr., T. Vreven, K. N. Kudin, J. C. Burant, J. M. Millam, S. S. Iyengar, J. Tomasi, V. Barone, B. Mennucci, M. Cossi, G. Scalmani, N. Rega, G. A. Petersson, H. Nakatsuji, M. Hada, M. Ehara, K. Toyota, R. Fukuda, J. Hasegawa, M. Ishida, T. Nakajima, Y. Honda, O. Kitao, H. Nakai, M. Klene, X. Li, J. E. Knox, H. P. Hratchian, J. B. Cross, C. Adamo, J. Jaramillo, R. Gomperts, R. E. Stratmann, O. Yazyev, A. J. Austin, R. Cammi, C. Pomelli, J. W. Ochterski, P. Y. Ayala, K. Morokuma, G. A. Voth, P. Salvador, J. J. Dannenberg, V. G. Zakrzewski, S. Dapprich, A. D. Daniels, M. C. Strain, O. Farkas, D. K. Malick, A. D. Rabuck, K. Raghavachari, J. B. Foresman, J. V. Ortiz, Q. Cui, A. G. Baboul, S. Clifford, J. Cioslowski, B. B. Stefanov, G. Liu, A. Liashenko, P. Piskorz, I. Komaromi, R. L. Martin, D. J. Fox, T. Keith, M. A. Al-Laham, C. Y. Peng, A. Nanayakkara, M. Challacombe, P. M. W. Gill, B. Johnson, W. Chen, M. W. Wong, C. Gonzalez, and J. A. Pople. (2003). *Gaussian 03, Revision B.04*. Pittsburgh: Gaussian Inc.